Surface-bound antigen induces B-cell permeabilization and lysosome exocytosis facilitating antigen uptake and presentation to T-cells

Fernando Y. Maeda[1#], Jurriaan J. H. van Haaren[1#], David B. Langley[2], Daniel Christ[2,3], Norma W. Andrews[1]* and Wenxia Song[1]*

[1]Department of Cell Biology and Molecular Genetics, University of Maryland, College Park, MD 20742, USA.

[2]Immunology Division, Garvan Institute of Medical Research, Darlinghurst, NSW 2010, Australia

[3]St Vincent's Clinical School, University of New South Wales, Darlinghurst, NSW 2010, Australia

[#]These authors contributed equally to this study.

*Co-corresponding authors:

Wenxia Song: wenxsong@umd.edu

Norma Andrews: andrewsn@umd.edu

Abstract

B-cell receptor (BCR)-mediated antigen internalization and presentation are essential for humoral memory immune responses. Antigen encountered by B-cells is often tightly associated with the surface of pathogens and/or antigen-presenting cells. Internalization of such antigens requires myosin-mediated traction forces and extracellular release of lysosomal enzymes, but the mechanism triggering lysosomal exocytosis is unknown. Here we show that BCR-mediated high-affinity recognition of antigen tethered to beads or planar lipid-bilayers causes localized plasma membrane (PM) permeabilization, a process that requires BCR signaling and non-muscle myosin II activity. B-cell permeabilization triggers a PM repair response involving lysosomal exocytosis. B-cells transiently permeabilized by surface-associated antigen internalize more antigen than cells that remain intact, and higher affinity antigens that cause more B-cell permeabilization and lysosomal exocytosis are more efficiently presented to T-cells. Thus, PM permeabilization by surface-associated antigen triggers a lysosome-mediated B-cell resealing response, which provides the extracellular hydrolases that can facilitate antigen internalization and presentation.

Introduction

B-cells are responsible for generating antibody responses that neutralize pathogens and attract immune cells. B-cell activation is initiated by the B-cell receptor (BCR), which surveys antigen through its membrane-anchored immunoglobulin (Reth 1994). Antigen-BCR interaction induces signaling cascades and antigen internalization, followed by intracellular processing and surface presentation to T-cells. Antigen presentation is essential for the activation of B-cells and their differentiation into high-affinity memory B-cells or antibody-secreting cells (Shlomchik and Weisel 2012). A property that is critical for maximizing humoral protection is the ability of clonal-specific BCRs to recognize antigen in different physical, chemical, and biological forms.

Antigen encountered by B-cells *in vivo* can be tightly associated with the surface of pathogens, such as parasites, bacteria and viruses, and/or antigen-presenting cells such as follicular dendritic cells (Gonzalez *et al.* 2011). Internalization, processing, and presentation of such surface-bound antigens are essential for specific B-cells to obtain T-cell help, which is critical for B-cell activation and differentiation. Follicular dendritic cells, which are uniquely present in germinal centers of the secondary lymphoid organs, acquire antigens that drain into these organs and present them as antibody- or complement-opsonized complexes (Suzuki *et al.* 2009; Cyster 2010). Competition between high and low-affinity B-cells to acquire antigen from follicular dendritic cells is a critical step in the selection of high-affinity B-cells that differentiate into memory B-cells and long-lived plasma cells.

B-cells, and follicular B-cells in particular, are thought to have a limited ability to phagocytose large insoluble antigen particles (Vidard *et al.* 1996). However, B-cells are able to extract and

endocytose antigen that is tightly associated with non-internalizable surfaces (Batista and Neuberger 2000). Importantly, the efficiency by which B-cells present antigen depends more strongly on the BCR-antigen binding affinity when the antigen is associated with non-internalizable surfaces, compared to antigen bound to particles that can be internalized (Batista and Neuberger 2000). Recent studies using antigen-coated beads, planar lipid bilayers, and/or plasma membrane (PM) sheets revealed two major mechanisms by which B-cells extract antigen from non-internalizable surfaces for endocytosis. Mechanical forces, generated by non-muscle myosin II (NMII) activation at sites of antigen-BCR interaction, can directly pull antigen from presenting surfaces for endocytosis. When mechanical forces alone are not sufficient, hydrolases released from lysosomes cleave surface-associated antigen to facilitate internalization (Yuseff *et al.* 2011; Natkanski *et al.* 2013; Spillane and Tolar 2017; Wang *et al.* 2018). Surface-associated antigen was previously shown to induce polarization of B-cell lysosomes towards antigen-binding sites (Yuseff *et al.* 2011), but the mechanism responsible for triggering lysosome exocytosis and release of hydrolytic enzymes was unknown.

When cells are permeabilized by physical tearing or by pore-forming proteins, Ca^{2+} influx triggers rapid exocytosis of lysosomes as part of the process that repairs the PM and prevents cell death (Reddy *et al.* 2001; Andrews *et al.* 2014). Since its discovery several decades ago (Rodríguez *et al.* 1997), Ca^{2+}-dependent lysosomal exocytosis has been observed in many cell types (Zhang *et al.* 2007; Naegeli *et al.* 2017; Villeneuve *et al.* 2018; Ibata *et al.* 2019). We previously reported that permeabilizing the PM of mouse splenic B-cells with the pore-forming toxin streptolysin O triggers lysosomal exocytosis, releasing lysosomal enzymes extracellularly and exposing the luminal epitope of the lysosome-associated protein LIMP-2 on the cell surface.

B-cells rapidly reseal these PM lesions, in a process that requires lysosomal exocytosis (Miller *et al.* 2015). Surprisingly, in this study we found that interaction of the BCR with surface-associated antigen can permeabilize the B-cell PM, triggering a resealing mechanism that involves exocytosis of lysosomes. We investigated this process by determining if antigen-induced PM permeabilization depends on BCR-antigen binding affinity, BCR signaling and NMII motor activity, and if it influences the ability of B-cells to internalize and present surface-associated antigens to T-cells.

Results

BCR interaction with surface-associated antigen induces B-cell PM permeabilization at antigen-binding sites

We utilized two experimental models extensively used previously to study BCR-mediated internalization of surface-associated antigen: F(ab')$_2$-anti-mouse IgM+G (αM, binding and activating mouse BCRs) and hen egg lysozyme (HEL, recognized by BCRs of MD4 mice) immobilized on beads or tethered to planar lipid bilayers (PLB) by biotin-streptavidin interaction. Beads or PLB coated with transferrin (Tf) at similar surface density were used as controls, as Tf does not activate the BCR and interacts with the Tf receptor with similar affinity as HEL-MD4 BCR interaction (Batista and Neuberger 1998; Fuchs and Gessner 2002). Strikingly, live-cell imaging revealed entry of the membrane-impermeable dye propidium iodide (PI) at the B-cell side in contact with αM-beads, indicating that PM permeabilization occurred at bead-binding sites (*Figure 1A, Figure 1-figure supplement 1, and Videos 1-3*). A significantly higher fraction of B-cells binding αM-beads than those binding Tf-beads became PI-positive, even though similar percentages of B-cells bound αM- or Tf-beads (*Figure 1B and C*). Flow

Figure 1

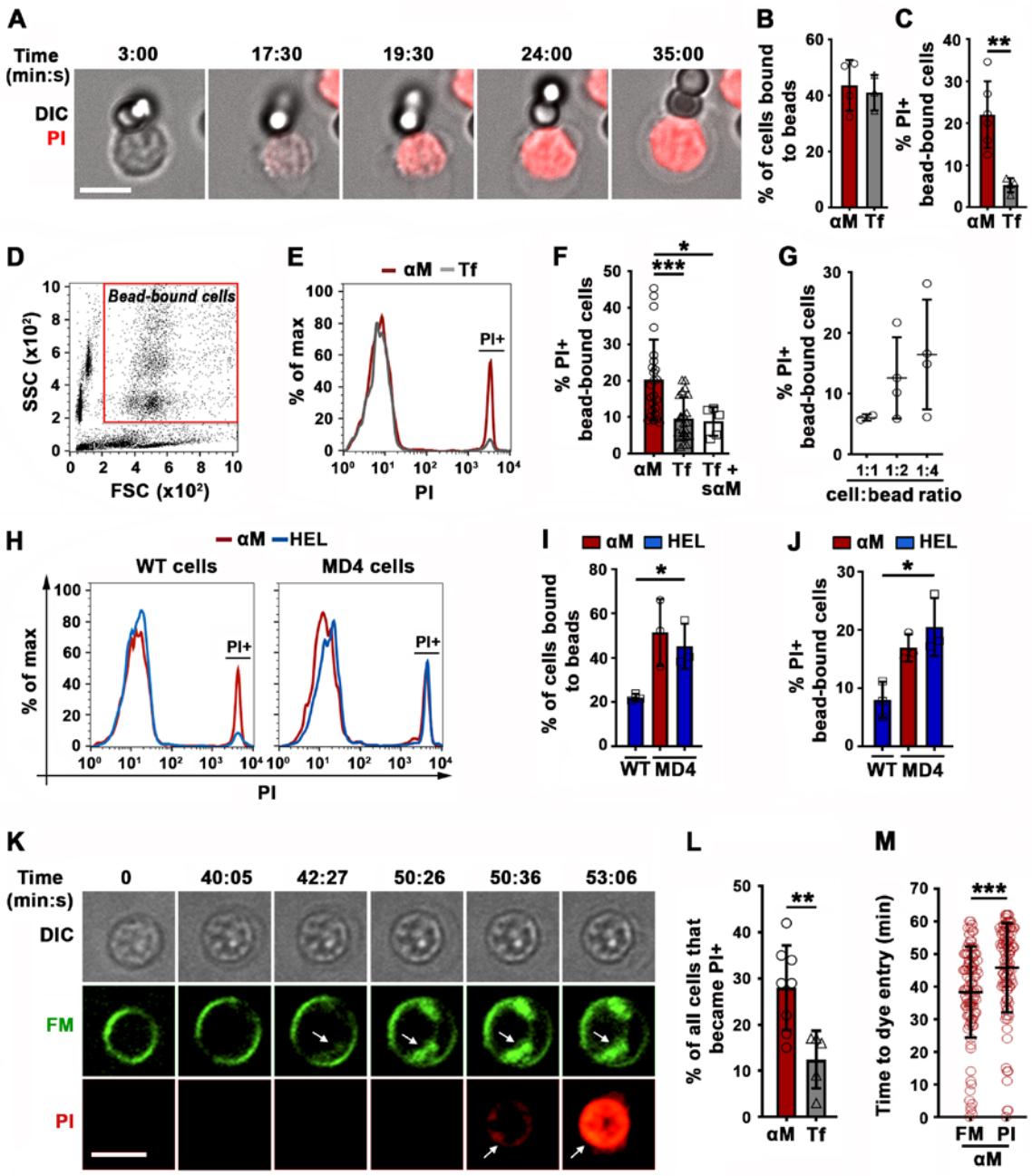
A
Time (min:s)
3:00
17:30
19:30
24:00
35:00
DIC
PI
B
% of cells bound to beads
αM
Tf
C
% PI+ bead-bound cells
**
D
Bead-bound cells
SSC (x10²)
FSC (x10²)
E
αM
Tf
% of max
PI+
PI
F
% PI+ bead-bound cells
***
*
Tf + sαM
G
% PI+ bead-bound cells
1:1
1:2
1:4
cell:bead ratio
H
αM
HEL
WT cells
MD4 cells
% of max
PI+
PI
I
% of cells bound to beads
WT
MD4
J
% PI+ bead-bound cells
K
Time (min:s)
0
40:05
42:27
50:26
50:36
53:06
DIC
FM
PI
L
% of all cells that became PI+
M
Time to dye entry (min)
FM
PI

105

Figure 1. BCR binding to surface-associated antigen causes B-cell PM permeabilization. (**A**) Spinning disk time-lapse images of a splenic B-cell incubated with αM-beads (1:2 cell:bead ratio) in the presence of PI (Movie S1). (**B**) Percentages of B-cells bound to beads. Data points represent independent experiments (mean ± SD). (**C**) Percentages of PI-positive (PI+) cells in bead-bound B-cells at 30 min quantified from the images. Data points represent independent experiments (mean ± SD). (**D**) Gate for bead-bound B-cells in a flow cytometry forward and side scatter dot plot. (**E**) Histograms of PI fluorescence intensity (FI) of αM- and Tf-bead-bound B-cells after 30 min incubation. (**F**) Percentages of PI+ bead-bound B-cells after 30 min incubation with αM- or Tf-beads in the presence or absence of soluble αM (sαM). Data points represent independent experiments (mean ± SD). (**G**) Percentages of PI+ bead-bound B-cells after 30 min with αM-beads at indicated cell:bead ratios. Data points represent independent experiments (mean ± SD). (**H**) Histograms of PI FI of WT or MD4 B-cells incubated with αM- or HEL-beads for 30 min. (**I**) Percentages of WT and MD4 B-cells binding αM- or HEL-beads. Data points represent independent experiments (mean ± SD). (**J**) Percentages of PI+ bead-bound WT or MD4 B-cells after 30 min incubation. Data points represent independent experiments (mean ± SD). (**K**) Spinning disk time-lapse images of a B-cell interacting with αM-PLB in the presence of FM1-43 and PI (Arrows, FM1-43 or PI entry, *Video 4*). (**L**) Percentages of PI+ B-cells interacting with αM- or Tf-PLB for 30 min. Data points represent independent experiments (mean ± SD). (**M**) PI or FM1-43 entry time in B-cells interacting with αM-PLB. Data points represent individual cells in three independent experiments (mean ± SD). Bars, 5 μm. *$p \leq 0.05$, **$p \leq 0.01$, ***$p \leq 0.005$, unpaired Student's *t*-test or one-way ANOVA.

Figure supplement 1. BCR binding to αM-beads causes localized PM permeabilization in B-cells.

Figure supplement 2. Identification of bead-bound B-cells by flow cytometry.

Figure supplement 3. BCR binding to αM-beads does not increase apoptosis in B-cells.

Figure supplement 4. Early detection of B-cell permeabilization by intracellular FM staining.

Figure supplement 5. The lipophilic FM dye enters B-cells permeabilized by surface-associated antigen, staining the nuclear envelope.

cytometry analysis confirmed the increased PI entry in B-cells binding αM-beads when compared to Tf-beads (*Figure 1D-G and Figure 1-figure supplement 2*). Addition of soluble $F(ab')_2$-anti-mouse IgM+G (sαM, capable of binding and activating the BCR) did not increase the frequency of PI entry in B-cells binding to Tf-beads (*Figure 1F*). The percentage of cells positive for cleaved caspase-3, an early apoptotic marker, was similar in B-cells interacting or not with αM- or Tf-beads, and only increased significantly after treatment with staurosporine (*Figure 1-figure supplement 3*). Flow cytometry analysis also revealed similar fractions of bead-bound MD4 B-cells becoming PI-positive after binding beads coupled to αM or to the *bona fide* antigen HEL (*Figure 1 H-J*). In contrast, WT B-cells binding to HEL-beads showed a low percentage of PI-positive cells, similar to those binding Tf-beads (*Figure 1F and J*). Similar observations were made using the PLB system that allows lateral movement of the tethered antigen (Dustin *et al.* 2007). Significantly more B-cells became PI-positive when contacting αM-PLB when compared to Tf-PLB (*Figure 1K and L*).

We confirmed that binding to surface-associated antigen induces B-cell PM permeabilization by using membrane-impermeable, fluorescent lipophilic FM probes. These dyes are used extensively for detecting PM permeabilization, because they only label the outer PM leaflet in intact cells but rapidly stain intracellular membranes when entering cells (Bansal *et al.* 2003; McNeil *et al.* 2003; Demonbreun *et al.* 2019). After >30 min of interaction with αM-PLB we observed sudden, massive increases in intracellular FM associated with intracellular structures, including the nuclear envelope (*Figure 1K, Figure 1-figure supplements 4 and 5, and Video 4*). Sudden FM influx was only observed in B-cells that eventually became PI-positive, but not in cells that remained PI-negative during interaction with αM-PLB. This observation, in addition to

the minimal amounts of intracellular FM dye detected in all B-cells prior to 30-40 min, indicate that the massive intracellular staining of B-cells interacting with αM-PLB is a result of PM permeabilization and extracellular dye influx, and not endocytosis. FM influx was detected on average ~8 min before nuclear staining with PI (*Figure 1K and M, Figure 1-figure supplements 4, and Video 4*). Thus, FM intracellular influx is a more sensitive method for detecting the onset of B-cell PM permeabilization when compared to PI, which can only be visualized after accumulating inside the nucleus and intercalating into DNA. Collectively, these results show that BCR binding to surface-associated antigen can cause localized permeabilization of the B-cell PM.

Antigen-induced B-cell permeabilization requires high-affinity BCR-antigen binding, BCR signaling, and NMII motor activity

Previous studies showed that high-affinity BCR-antigen binding induce high levels of BCR signaling, cytoskeleton reorganization, and endocytosis of antigen bound to non-internalizable surfaces (Batista and Neuberger 1998; Batista and Neuberger 2000; Fleire *et al.* 2006). To examine the impact of BCR binding affinity on antigen-induced PM permeabilization, we incubated MD4 B-cells with beads coated with equal densities of HEL or the duck egg lysozyme isoform DEL-I. The MD4 BCR binds DEL-I with >100 fold lower affinity than it binds HEL (Langley *et al.* 2017). As expected, the percentage of B-cells binding to multiple beads was reduced when the BCR-antigen affinity decreased, but B-cells binding one single bead were detected with both HEL and DEL-I, and also Tf (*Figure 2-figure supplement 1*). In these single bead-bound populations, DEL-I-beads caused significantly less PI entry than HEL-beads (*Figure 2A*). Signaling inhibition with non-toxic concentrations of the Src kinase inhibitor PP2 (Cheng *et*

Figure 2

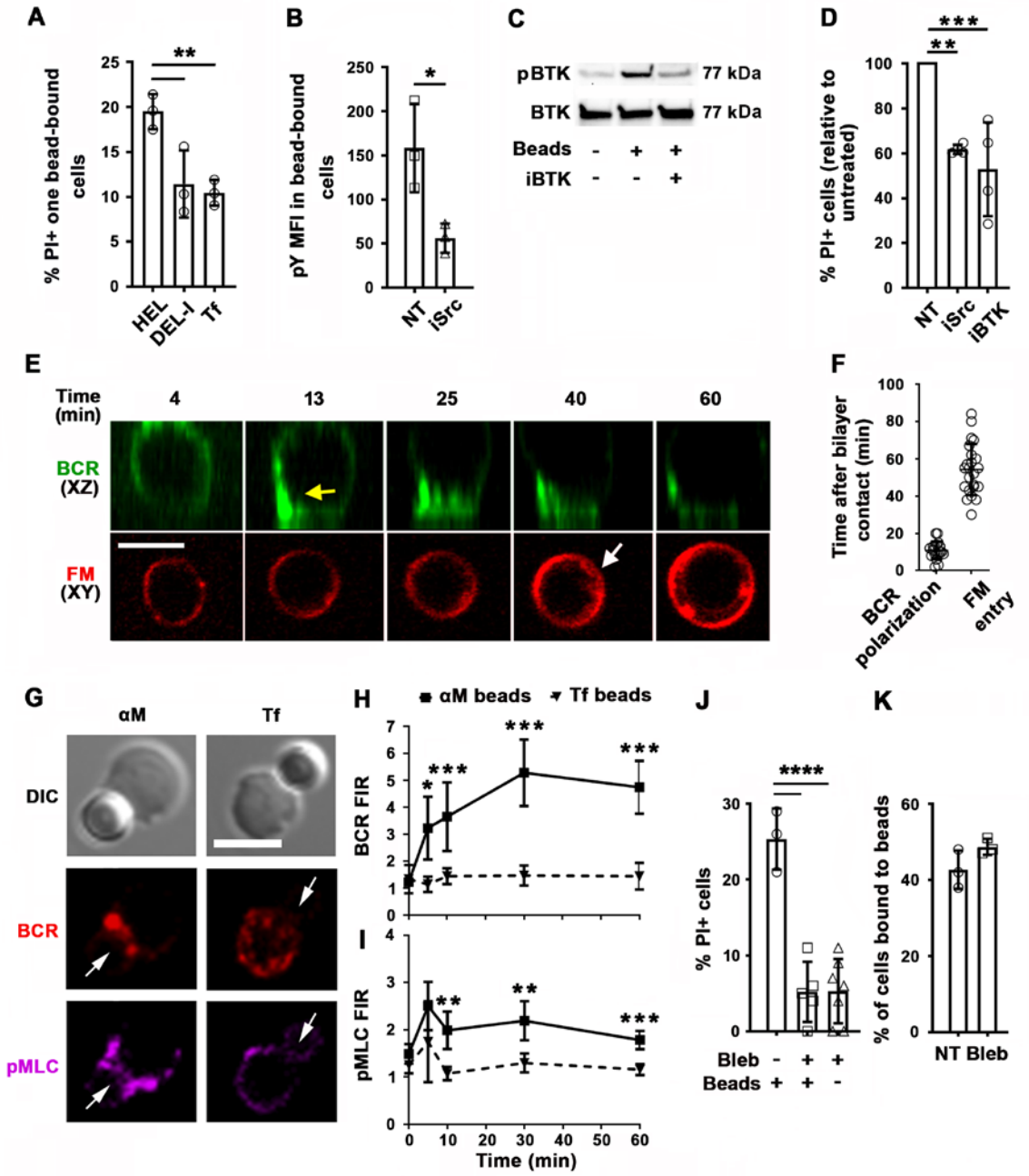
A
% PI+ one bead-bound cells
HEL
DEL-I
Tf
B
pY MFI in bead-bound cells
NT
iSrc
C
pBTK
BTK
77 kDa
Beads
iBTK
D
% PI+ cells (relative to untreated)
NT
iSrc
iBTK
E
Time (min)
BCR (XZ)
FM (XY)
F
Time after bilayer contact (min)
BCR polarization
FM entry
G
αM
Tf
DIC
BCR
pMLC
H
αM beads
Tf beads
BCR FIR
I
pMLC FIR
Time (min)
J
% PI+ cells
Bleb
Beads
K
% of cells bound to beads
NT
Bleb

181

Figure 2. PM permeabilization induced by surface-associated antigen depends on high-affinity BCR-antigen binding, BCR signaling, and non-muscle myosin II (NMII) motor activity. (**A**) Percentages of PI+ single bead-binding B-cells after incubation with HEL-, DEL-I- or Tf-beads (1:4 cell:bead ratio) for 30 min. Data points represent independent experiments (mean ± SD). (**B**) Mean fluorescence intensity (MFI) of phosphotyrosine (pY) in HEL-bead-bound B-cells treated or untreated (NT) with a Src kinase inhibitor (iSrc) by flow cytometry. Data points represent independent experiments (mean ± SD). (**C***)* Western blot analysis of pBTK and BTK in B-cells incubated with HEL-beads in the presence or absence of BTK inhibitor (iBTK) for 30 min. (**D**) Percentages of PI+ HEL-bead-bound cells treated with iSrc or iBTK relative to NT at 30 min. Data points represent independent experiments (mean ± SD). (**E**) Spinning disk time-lapse images of BCR polarization (yellow arrow) in a B-cell incubated with αM-PLB in the presence of FM4-64 (white arrow, intracellular FM). (**F**) Timing of BCR polarization and FM entry of individual cells interacting with αM-PLB. Data points represent individual cells in three independent experiments (mean ± SD). (**G**) Confocal images of BCR and phosphorylated NMII light chain (pMLC) staining in B-cells interacting with αM- or Tf-beads (Arrows, bead binding sites). (**H** and **I**) Mean fluorescence intensity ratio (FIR) of BCR (**H**) and pMLC (**I**) staining at the bead-binding site relative to the opposite PM in αM- and Tf-bead-bound cells over time. Data represent the averages of three independent experiments (mean ± SD). (**J**) Blebbistatin effect on B-cell permeabilization. Data points represent percentages of PI+ cells in individual videos from three independent experiments (mean ± SD). (**K**) Percentages of bead-bound B-cells incubated with αM-beads for 30 min in the presence or absence of blebbistatin (Bleb). Data points represent independent experiments (mean ± SD). Bar, 5 μm. *$p \leq 0.05$, **$p \leq 0.01$, ***$p \leq 0.005$, ****$p \leq 0.001$, unpaired Student's *t*-test or one-way ANOVA.

Figure supplement 1. Impact of BCR-antigen affinity on B-cell-bead binding.

Figure supplement 2. B-cell binding to αM-PLB but not to Tf-PLB triggers BCR polarization first and PM permeabilization later.

Figure supplement 3. BCR and phosphorylated myosin light chain (pMLC) polarize towards αM-bead binding sites.

al. 2001) (iSrc) or the Bruton's Tyrosine Kinase inhibitor AVL-292 (Aalipour and Advani 2013) (iBTK) (*Figure 2B and C*) also reduced PI entry in cells binding HEL-beads (*Figure 2D*). Following contact with αM-PLB or αM-beads but not Tf-PLB or Tf-beads, surface BCRs became polarized (measured using image analysis software) towards PLB- or bead-binding sites within ~10 min, a period markedly shorter than what was required for the onset of PM permeabilization, detected through FM influx (*Figure 2E-H, Figure 2-figure supplements 2 and 3, and Video 5*). Similarly, the activated form of the actin motor protein NMII, detected through its phosphorylated light chain (pMLC), accumulated along with the BCR at αM-bead-binding sites (*Figure 2G, Figure 2-figure supplement 3, and Video 6*). The fluorescence intensity ratios (FIR) of both surface BCRs and pMLC in B-cells binding αM-beads were significantly higher than those binding Tf-beads (*Figure* 2*H and I*). Importantly, inhibition of NMII motor activity with blebbistatin (Bleb) markedly reduced the number of B-cells that became PI-positive during interaction with αM-beads, without affecting the cells' ability to bind the beads (*Figure 2J and K*). Live-imaging detected PI entry following a "tug-of-war' between two B-cells simultaneously engaging an αM-bead (*Video 3 and Figure 1-figure supplement 1C*), further supporting a role for NMII-mediated traction forces in antigen-induced PM permeabilization. These data suggest that PM permeabilization caused by surface-associated antigen requires strong BCR-antigen interaction and the subsequent activation of signaling and NMII motor activity.

Antigen-induced B-cell permeabilization triggers lysosome exocytosis as a repair response

We previously showed that permeabilizing B-cells with the pore-forming toxin streptolysin O triggers lysosomal exocytosis (Miller *et al.* 2015), a response required for sealing PM wounds (Reddy *et al.* 2001). In this study, we found that B-cells permeabilized during interaction with

surface-associated antigen also rapidly reseal their PM, by utilizing an assay involving sequential exposure to the membrane impermeable dyes FM4-64 and SYTOX Blue. Repaired cells were quantified by flow cytometry as the percentage of permeabilized αM-bead-binding cells (stained intracellularly with FM4-64 kept throughout the assay) that excluded the membrane-impermeable dye SYTOX Blue added during the last 10 min of the assay (*Figure 3A*). The inhibitor of lysosomal exocytosis bromoenol lactone (BEL) (Fensome-Green *et al.* 2007; Tam *et al.* 2010) significantly reduced the percentage of resealed cells (*Figure 3B*) while not increasing the numbers of dead cells, detected as low forward- and side-scatter populations by flow cytometry (*Figure 3-figure supplement 1*). These data suggested that lysosomal exocytosis is required for the resealing of B-cells permeabilized by binding to surface-associated antigen.

To directly determine if PM permeabilization by surface-associated αM or HEL triggers lysosome exocytosis in B-cells, we utilized two independent methods: Surface exposure of luminal epitopes of the lysosomal membrane protein LIMP-2 and live total internal reflection fluorescence microscopy (TIRF). Flow cytometry analysis detected surface LIMP-2 in a higher percentage of B-cells binding αM-beads than in B-cells binding Tf-beads (*Figure 3C and D*). Notably, surface exposure of LIMP-2 was lower in MD4 B-cells binding DEL-I-beads compared to HEL-beads (*Figure 3E*). These results show a close correlation between the extent of PM permeabilization (*Figure 2A*) and lysosomal exocytosis induced by surface-associated αM and HEL/DEL-I (*Figure 3D-E*). Surface LIMP-2 was predominantly detected at sites of αM-bead binding (*Figure 3F and Figure 3-figure supplement 2*) and this polarized pattern, measured by FIR, increased after ~30 min of interaction with αM- but not Tf-beads (*Figure 3G*), a timeframe similar to the period required for PM permeabilization (*Figure 1M*). Using TIRF microscopy, we

Figure 3

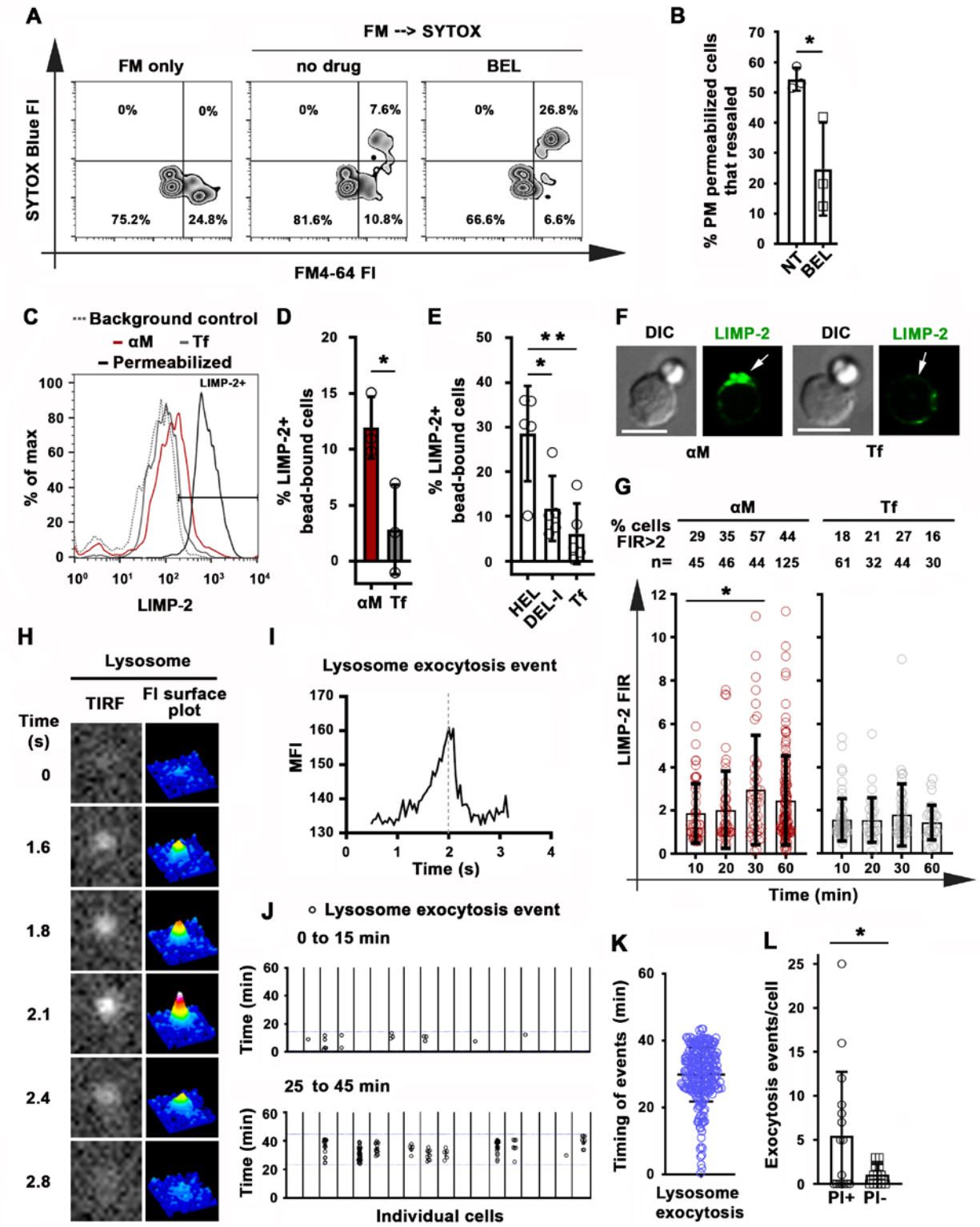
A
FM --> SYTOX
FM only
no drug
BEL
SYTOX Blue FI
FM4-64 FI
0%
0%
75.2%
24.8%
0%
7.6%
81.6%
10.8%
0%
26.8%
66.6%
6.6%
B
% PM permeabilized cells that resealed
NT
BEL
C
Background control
αM
Tf
Permeabilized
LIMP-2+
% of max
LIMP-2
D
% LIMP-2+ bead-bound cells
αM
Tf
E
% LIMP-2+ bead-bound cells
HEL
DEL-I
Tf
F
DIC
LIMP-2
DIC
LIMP-2
αM
Tf
G
αM
Tf
% cells FIR>2
29 35 57 44
18 21 27 16
n=
45 46 44 125
61 32 44 30
LIMP-2 FIR
Time (min)
H
Lysosome
TIRF
FI surface plot
Time (s)
0
1.6
1.8
2.1
2.4
2.8
I
Lysosome exocytosis event
MFI
Time (s)
J
Lysosome exocytosis event
0 to 15 min
25 to 45 min
Time (min)
Individual cells
K
Timing of events (min)
Lysosome exocytosis
L
Exocytosis events/cell
PI+
PI-

257

Figure 3. Antigen-induced permeabilization triggers PM repair mediated by lysosomal exocytosis. (**A**) Resealed bead-bound B-cells after incubation with αM-beads were assessed by flow cytometry analysis of FM4-64 (added at the start) and SYTOX Blue (added in the last 10 min) fluorescence intensity (FI) in the presence or absence of BEL. (**B**) Percentages of permeabilized αM-bead-bound cells that resealed in the presence or absence of BEL. Data points represent independent experiments (mean ± SD). (**C**) Flow cytometry analysis of surface-exposed (no detergent permeabilization) and/or intracellular LIMP-2 (with detergent permeabilization) of bead-bound B-cells after incubation with αM- or Tf-beads for 30 min. (**D** and **E**) Percentages of surface-exposed LIMP-2 (relative to values obtained with secondary antibody alone) in bead-bound B-cells incubated with αM- or Tf-beads (**D**) or with HEL-, DEL-I- or Tf-beads for 30 min (**E**). Data points represent independent experiments (mean ± SD). (**F**) Confocal images of surface-exposed LIMP-2 in B-cells incubated with αM- or Tf-beads (Arrows, bead-binding sites). Bars, 5 μm. (**G**) FIR (bead-binding site:opposite PM) of surface-exposed LIMP-2 in individual cells over time. Data points represent individual cells (mean ± SD). (**H**) Total internal reflection microscopy (TIRF) images (left column) and FI surface plots (right column) of SiR-Lyso at the B-cell surface contacting αM-PLB. (**I**) Representative MFI versus time plot of a SiR-Lyso-loaded lysosome undergoing exocytosis. (**J**) SiR-Lyso exocytosis events (circles) in individual B-cells during the first 0-15 min or 25–45 min of incubation with αM-PLB. (**K**) Times of individual SiR-Lyso exocytosis events in B-cells incubated with αM-PLB during a 45 min incubation. Data points represent individual cells from three independent experiments (mean ± SD). (**L**) Numbers of SiR-Lyso exocytosis events per B-cell permeabilized (PI+) or not permeabilized (PI-) by αM-PLB during a 45 min incubation. Data points represent individual cells from three independent experiments (mean ± SD). *$p \leq 0.05$, **$p \leq 0.01$, unpaired Student's *t*-test or one-way ANOVA.

Figure supplement 1. Bromoenol lactone (BEL) does not affect B-cell viability.

Figure supplement 2. BCR-mediated binding of αM-beads induces surface exposure of the LIMP-2 luminal domain at bead contact sites.

Figure supplement 3. Detection of lysosomal exocytosis by total internal reflection fluorescence (TIRF) microscopy.

imaged live B-cells preloaded with a specific lysosome probe (SiR-lyso, a membrane-permeable fluorescent dye conjugated to a peptide that binds the lysosomal enzyme cathepsin D) while contacting αM-PLB. Exocytosis events were identified by rises in the fluorescence intensity of SiR-lyso puncta (reflecting lysosome entry into the TIRF evanescent field adjacent to the PM) followed by sharp decreases within ~2 s (indicating dye dispersion upon fusion) (*Figure 3H and I, Figure 3-figure supplement 3, and Video 7*). Exocytosis events were observed in the majority of individual PI+ cells interacting with αM-PLB (*Figure 3J*) and occurred predominantly ~30-45 min after αM-PLB contact (*Figure 3J and K*), a timing similar to PM permeabilization and LIMP-2 exposure. Importantly, lysosomal exocytosis events were significantly more frequent in permeabilized B-cells when compared to B-cells that remained intact (*Figure 3L*). Thus, permeabilization of B-cells by surface-associated αM triggers localized lysosomal exocytosis at antigen-BCR interaction sites as a PM repair response.

B-cell permeabilization and lysosome exocytosis facilitate internalization and presentation of surface-associated antigen

Next we investigated the relationship between PM permeabilization by surface-associated antigen and antigen internalization, using fluorescent αM covalently bound to beads or tethered to PLB. Live-cell imaging detected αM puncta moving away from bead-binding sites into B-cells, increasing progressively between 30 and 60 min of interaction (*Figure 4A and B and Video 8*). In contrast, intracellular fluorescent puncta were markedly less abundant during the same time period in cells not binding αM-beads, or binding Tf-beads (*Figure 4B*). Importantly, inhibition of antigen-mediated PM permeabilization with blebbistatin significantly reduced extraction and internalization of αM coupled to beads (*Figure 4C*). When similar experiments

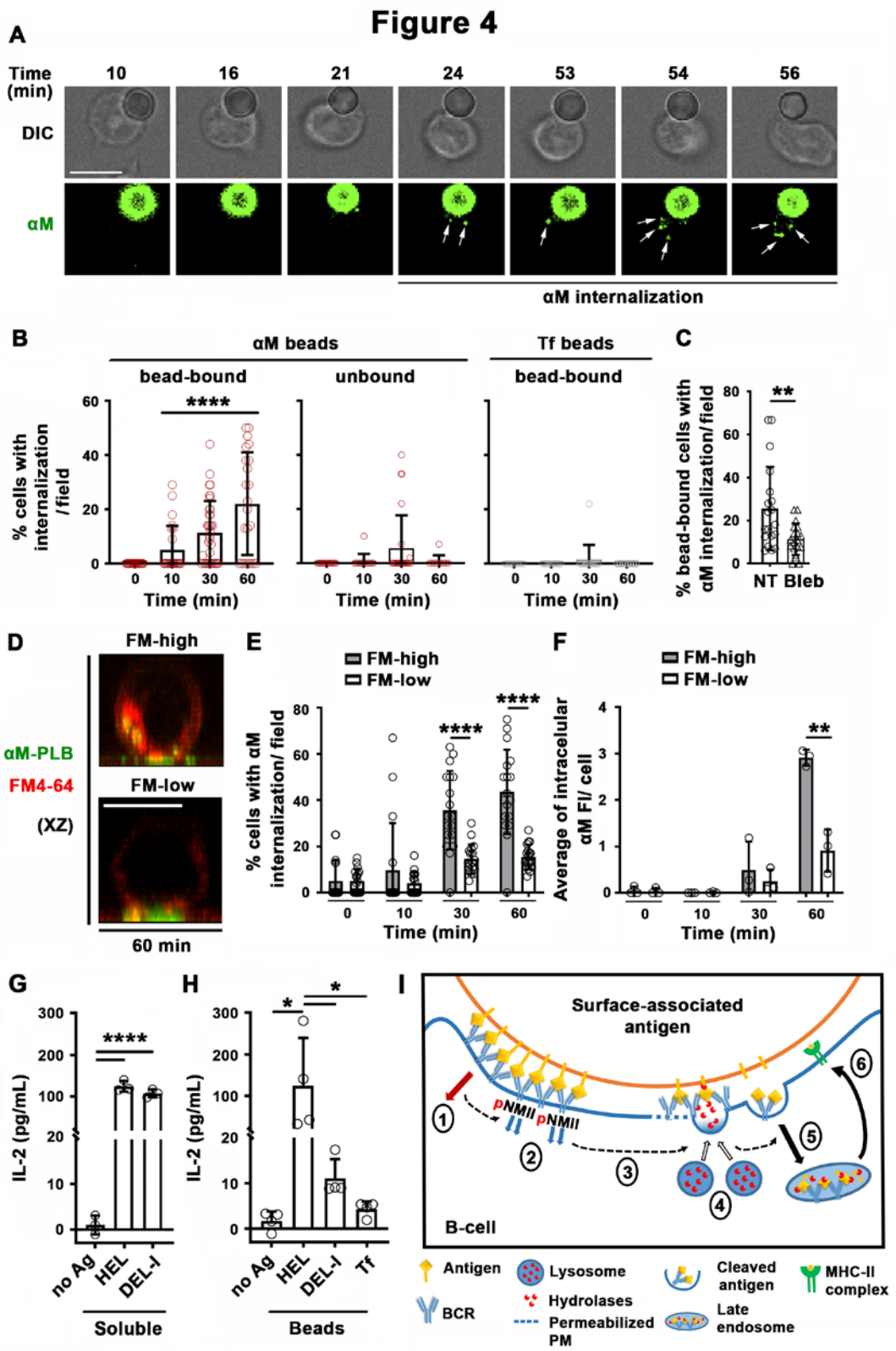
Figure 4
A
Time (min)
10
16
21
24
53
54
56
DIC
αM
αM internalization
B
αM beads
Tf beads
bead-bound
unbound
bead-bound
% cells with internalization / field
****
Time (min)
C
% bead-bound cells with αM internalization/ field
**
NT
Bleb
D
FM-high
FM-low
αM-PLB
FM4-64
(XZ)
60 min
E
FM-high
FM-low
% cells with αM internalization/ field
****
****
Time (min)
F
FM-high
FM-low
Average of intracelular αM FI/ cell
**
Time (min)
G
IL-2 (pg/mL)
****
no Ag
HEL
DEL-I
Soluble
H
IL-2 (pg/mL)
*
*
no Ag
HEL
DEL-I
Tf
Beads
I
Surface-associated antigen
pNMII
pNMII
B-cell
Antigen
BCR
Lysosome
Hydrolases
Permeabilized PM
Cleaved antigen
Late endosome
MHC-II complex

311

Figure 4. Antigen-induced PM permeabilization promotes antigen internalization and presentation. (**A**) Confocal live imaging of a B-cell interacting with fluorescent αM-beads (Arrows, internalized αM). (**B**) Percentages of cells containing internalized αM or Tf, bound or not to αM- or Tf-beads, over time. Data points represent individual fields in three independent experiments (mean ± SD). (**C**) Percentages of bead-bound B-cells with internalized αM in the presence or absence of Bleb after 60-min incubation. Data points represent individual fields in three independent experiments (mean ±SD). (**D**) Confocal images (xz) of αM internalization in B-cells permeabilized (FM-high) or not permeabilized (FM-low) by αM-PLB after 60-min incubation. (**E**) Percentages of B-cells permeabilized (FM-high) or not permeabilized (FM-low) by αM-PLB containing internalized αM over time. Data points represent individual fields in three independent experiments (mean ± SD). (**F**) MFI of internalized αM in individual B-cells permeabilized (FM-high) or not permeabilized (FM-low) by αM-PLB over time. Data points represent independent experiments (mean ± SD). (**G**) IL-2 secretion by 3A9 T-cells activated by B-cells incubated with or without (no Ag) soluble HEL or DEL-I (10 µg/ml) for 72 h. Data points represents independent experiments (mean ± SD). (**H**) IL-2 secretion by 3A9 T-cells activated by B-cells incubated with or without HEL-, DEL-I- or Tf-beads (1:4 cell:bead ratio) for 72 h. Bar, 5 µm. Data points represents independent experiments (mean ± SD). *$p \leq 0.05$, **$p \leq 0.01$, ****$p \leq 0.0001$, unpaired Student's *t*-test or one-way ANOVA. (**I**) Cartoon depicting the spatiotemporal relationship of events initiated by interaction of the BCR with surface-associated antigen. Our results enabled us to establish a working model. High-affinity binding stabilizes BCR-antigen bonds and induces strong BCR signaling (1) and NMII activation (2). Activated NMII generates local traction forces that permeabilize the PM (3), which triggers a localized PM repair response mediated by lysosomal exocytosis. Lysosome exocytosis releases hydrolases that can cleave antigen off surfaces (4), facilitating endocytosis (5) and presentation to T-cells (6).

were performed with PLB, the fraction of cells containing internalized αM and the total amount of αM uptake were significantly higher in permeabilized cells, identified by high levels of FM staining (FM-high), compared to non-permeabilized cells with low FM staining (FM-low) (*Figure 4D-F*). Collectively, these data suggest that αM-induced PM permeabilization, rapidly followed by lysosomal exocytosis, promotes extraction and internalization of αM from non-internalizable surfaces.

Next, we investigated whether antigen internalization enhanced by PM permeabilization and lysosome exocytosis impacts antigen presentation by B-cells. We compared the levels of IL-2 secretion by the 3A9 T-cell hybridoma line (Allen and Unanue 1984) after activation by B-cells exposed to bead-bound HEL or DEL-I. B-cells exposed to a high concentration of soluble HEL or DEL-I induced similar levels of IL-2 secretion (*Figure 4G*), demonstrating that the primary B-cells used in these assays could process and present the conserved peptide present in both HEL and DEL-I for T-cell activation. In contrast, when the B-cells were exposed to lower amounts of surface-associated antigens, B-cells exposed to HEL-beads activated T-cells to produce IL-2 at markedly higher levels compared to cells exposed to DEL-I-beads *(Figure 4H*). These results suggest that B-cell permeabilization resulting from high-affinity antigen-BCR interaction, with its corresponding lysosomal exocytosis response, facilitates the presentation of antigen associated with non-internalizable surfaces.

Discussion

Extracellular release of lysosomal enzymes by B-cells was previously proposed to cleave antigens tightly associated with non-internalizable surfaces, facilitating their internalization and presentation to T-cells (Yuseff *et al.* 2011; Spillane and Tolar 2017). However, it was unclear what the mechanism was responsible for inducing lysosomal enzyme release when B-cells engaged such insoluble antigen. In this study we show that interaction of the BCR with surface-associated antigen can cause permeabilization of the B-cell PM, triggering lysosomal exocytosis as part of the PM repair response (Rodríguez *et al.* 1997; Reddy *et al.* 2001). The antigen-dependent PM permeabilization occurs at antigen-binding sites, and is reversible under conditions that allow lysosomal exocytosis. We further demonstrate that PM permeabilization and lysosomal exocytosis require high-affinity binding of the BCR to antigen, BCR signaling, activation of NMII motor activity, and promote antigen internalization and presentation. Thus, our study identifies a critical novel step in the affinity-dependent process by which B-cells capture antigen tightly associated with surfaces, for effective internalization and subsequent presentation to T-cells.

Capture and internalization of antigen tightly associated with surfaces is an immunologically important process, as B-cells encounter this type of antigen *in vivo* on parasites, bacteria, and viruses, as well as on immune cells such as follicular dendritic cells. Follicular dendritic cells capture antigen drained into lymph nodes and present it on their surface to germinal center B-cells. In this manner, follicular dendritic cells enhance BCR antigenic stimulation by increasing antigen avidity, in addition to providing costimulatory molecules (Natarajan *et al.* 2001). While the exact percentage is unknown, studies have suggested that the majority of antigen that B-cells

encounter *in vivo* are in a membrane-associated form (Batista and Harwood 2009). Importantly, the capture, internalization, and presentation of such surface-associated antigens to T-cells are essential for selecting specific B-cells for survival, clonal expansion, and differentiation into long-lived high-affinity memory B-cells and antibody-secreting cells (Gitlin *et al.* 2014).

We found that B-cell PM permeabilization induced by surface-associated antigen depends on the motor activity of NMII. Following BCR polarization, activated NMII accumulates at sites of B-cell binding to αM- or HEL-beads or PLB before PM permeabilization occurs. These findings are consistent with previous studies showing that internalization of surface-associated but not soluble antigen requires NMII-mediated traction forces at antigen-binding sites (Natkanski *et al.* 2013; Spillane and Tolar 2018). Our results support the notion that NMII-mediated traction forces generated during BCR-antigen interaction are responsible for B-cell PM permeabilization. Whether this permeabilization is due to tearing of the membrane (Andrews *et al.* 2014) or the opening of mechanosensitive ion channels (Liu *et al.* 2018; Liu and Ganguly 2019) is currently unknown. However, the number of permeabilized B-cells that were able to reseal was reduced when lysosomal exocytosis, a component of the PM resealing response (Reddy *et al.* 2001), was inhibited - suggesting that NMII-mediated membrane tearing is the mechanism underlying antigen-dependent B-cell PM permeabilization.

We detected B-cell PM permeabilization during interaction with surface-associated antigen by following the entry of membrane-impermeable DNA-binding or lipophilic dyes. While the two types of dyes bind to different intracellular structures, both showed sudden rather than gradual increases in intracellular staining, consistent with PM permeabilization rather than dye

endocytosis. Strengthening this conclusion, FM lipophilic dyes rapidly associated with the nuclear envelope in a kinetics that was closely followed by PI nuclear staining. Not all cells binding surface-associated antigen were permeabilized, possibly as a result of the heterogeneity of the B-cell population. Splenic B-cells are found at different stages of peripheral maturation and differentiation (Sagaert and De Wolf-Peeters 2003; Allman and Pillai 2008), thereby binding antigen with variable affinity and at different times. It will be interesting to examine further which subsets of B-cells are more effective in capturing and presenting surface-associated antigen through NMII-dependent PM permeabilization.

The rapid exocytosis of lysosomes triggered by B-cell permeabilization that was uncovered in our study provides a mechanistic explanation for previously reported affinity-dependent extraction and presentation of antigen associated with non-internalizable surfaces (Batista and Neuberger 2000). We showed that DEL-I, which binds the MD4 BCR with a 100-fold lower affinity than HEL, induces markedly lower levels of PM permeabilization, lysosome exocytosis, and antigen presentation than HEL, when both antigens are displayed on beads and PLB at similar densities. Surface association significantly enhances the avidity of antigens by increasing their valency, a process that can reduce the impact of BCR-binding affinity on BCR signaling, antigen internalization and presentation when compared to soluble forms of the same antigen. However, this avidity effect is primarily observed with antigen associated to surfaces that B-cells are able to internalize (Batista and Neuberger 2000), and it is known that B-cell subsets such as native follicular B-cells have very low phagocytic capacity (Vidard *et al.* 1996). We envision that when antigen is strongly associated with non-internalizable surfaces, low-affinity BCR-antigen interactions are disrupted before B-cells can extract antigen. In this scenario, high-

affinity BCR interactions would be critical for sustaining antigen binding under NMII-mediated traction forces that promote PM permeabilization, lysosomal enzyme release, and antigen extraction. High-affinity BCR-antigen binding is also expected to induce more robust signaling than low-affinity binding, enabling higher levels of NMII activation (Fleire *et al.* 2006; Natkanski *et al.* 2013) and polarization to drive PM permeabilization. Collectively, in addition to supporting the notion that tight antigen attachment to non-internalizable surfaces facilitates B-cell affinity discrimination, our results expand the mechanistic understanding of why different physical and chemical forms (size, solubility, geometry, and molecular patterns) of immunogens impact the efficacy of vaccines (Bachmann and Jennings 2010; Khan *et al.* 2015).

Our study also provides important insight into the spatiotemporal relationship of events initiated by interaction of the BCR with surface-associated antigen (*Figure 4I*). Our results suggest that high-affinity binding stabilizes BCR-antigen bonds, inducing strong BCR signaling and NMII activation to locally generate traction forces that permeabilize the PM. Ca^{2+} entry then triggers a localized PM repair response mediated by lysosomal exocytosis, releasing hydrolases that can cleave antigen off surfaces, facilitating endocytosis and presentation to T-cells. Thus, our results support the notion that B-cells utilize a cellular mechanism that evolved for surviving PM injury to promote the acquisition, presentation, and possibly affinity discrimination of surface-associated antigens.

Materials and Methods

Key resources table

Reagent type (species) or resource	Designation	Source or reference	Identifiers	Additional information
Primary cell (spleen - C57BL/6)	WT	Jackson Laboratories	000664	
Primary cell (spleen - C57BL/6-Tg(IghelMD4)4Ccg/J)	MD4	Jackson Laboratories	002595	
Primary cell (spleen B10.BR-H2^{K2} H2-T18^{a}/ SgSnJJrep	B10.BR-H2^{K2} H2-T18^{a}/ SgSnJJrep	Jackson Laboratories	004804	
Cell line (Mus musculus)	A20	ATCC	TIB-208	B-cell lymphoma
Cell line (Mus musculus)	3A9	ATCC	CRL-3293	T-cell hybridoma
Reagent	Latex NH_2-beads	Polysciences	17145-5	
Ligand	αM (F(ab')$_2$ goat-anti-mouse IgM+G)	Jackson Immune Research	115-006-068	Binds to BCR
Antigen	HEL (Hen egg lysozyme)	Sigma-Aldrich	L6876	Binds to BCR from MD4 mice
Antigen	DEL-1 (Duck egg lysozyme)	David B. Langley and Daniel Christ laboratory		Binds to BCR from MD4 mice
Ligand	Tf (Holo- transferrin)	Sigma-Aldrich	T0665-50MG	Binds to transferrin receptor
Ligand	AF488-αM	Jackson Immune Research	115-546-003	Binds to BCR
Ligand	AF488-Tf	Thermo Fisher Scientifc	T13342	Binds to transferrin receptor
Commercial kit	BCA kit	Thermo Fisher Scientific	23235	Protein measurement during bead preparation
Control for antigen	Biotinylated transferrin (Tf-PLB)	Sigma-Aldrich	T3915-5MG	

Reagent	Streptavidin-conjugated Yellow-Green latex beads	Polyscience	24159-1	
Ligand	Biotin-SP (long spacer)-conjugated Fab fragments of goat-anti-mouse IgG (H+L)	Jackson Immune Research	115-067-003	
Inhibitor	Bleb (Blebbstatin)	Sigma-Aldrich	B0560	50 µM
Antibody	anti-phosphotyrosine mAb 4G10	Millipore	05-321	1:500
Antibody	AF488-goat-anti-mouse IgG_{2b}	Thermo Fisher Scientific	A-21141	
Reagent	PI (Propidium iodide)	Sigma-Aldrich	P4170-10MG	50 µg/ml
Reagent	FM1-43FX	Thermo Fisher Scientific	F35355	10 µg/ml
Reagent	FM4-64FX	Thermo Fisher Scientific	F34653	10 µg/ml
Reagent	SYTOX™ Blue nucleic acid stain	Invitrogen	S11348	300 nM
Inhibitor	Staurosporine	Abcam	120056	Apoptosis induction (1 µM)
Antibody	Cleaved Caspase-3 (Asp175) Antibody	Cell Signaling	9661T	1:500
Antibody	Cy5-Fab donkey-anti mouse IgG	Jackson ImmunoResearch	715-175-151	5 µg/ml
Antibody	Donkey anti-Rabbit IgG (H+L) Highly cross-adsorbed secondary antibody, Alexa Fluor 488	Thermo Fisher Scientific	A-21206	1:200
Inhibitor	PP2	Millipore-Sigma	529573	Src kinase inhibitor (5 µM)
Inhibitor	AVL-292	Selleckchem	S7173	BTK inhibitor (10 nM)
Antibody	anti-BTK	Cell Signaling	8547	1:1000
Antibody	Rabbit anti-phospho-BTK	Abcam	68217	1:500
Antibody	HRP goat-anti-rabbit	Jackson Immune Research	111-035-144	1:1000
Antibody	Cy3-Fab donkey-anti–mouse IgM+G	Jackson Immune Research	115-165-166	1:200

Antibody	Rabbit anti-phosphorylated myosin light chain (pMLC)	Cell Signaling	3671S	1:50
Antibody	AF633-goat-anti-rabbit IgG	Invitrogen	A-21070	1:500
Inhibitor	BEL (Bromoenol lactone)	Sigma-Aldrich	B1552	12 µM
Commercial kit	SiR-Lysosome and Verapamil	Cytoskeleton	CY-SC012	Lysosome probe 1 µM and 10 µM
Antibody	Rabbit-anti-LIMP-2	Sigma-Aldrich	SAB3500449-100UG	1:200
Antibody	AF488 donkey-anti-rabbit IgG	Life technology	A32790	1:200
Commercial kit	IL-2 ELISA kit	Biolegend	431804	
Software	FlowJo 10.1	FlowJo, LLC		https://www.flowjo.com/solutions/flowjo/downloads
Software	Volocity Suite	PerkinElmer		https://ir.perkinelmer.com/news-releases/news-release-details/perkinelmer-launches-volocityr-60-high-performance-3d-cellular
Software	NIH Image J			https://imagej.nih.gov/ij/
Software	MATLAB	MathWorks		https://www.mathworks.com/products/matlab.html
Software	Prism	GraphPad		https://www.graphpad.com/scientific-software/prism/
Antibody	Anti-CD90.2	Biolegend	105310	1 µl/ $2x10^6$ cells
Reagent	Guinea pig complement	Innovative Research	IGGPCSER	100 µl/ $4x10^7$ cells
Reagent	1,2-dioleoyl-sn-glycero-3-phosphocholine	Avanti Polar Lipids	850375P	5 mM (PLB)
Reagent	1,2-dioleoyl-sn-glycero-3-phosphoethanolamine-cap-biotin	Avanti Polar Lipids	870273C	50 µM (PLB)

448

Mice, B-cell isolation, and culture

Primary B-cells were isolated from the spleens of wild type C57BL/6, MD4 transgenic (C57BL/6 background), B10.BR-*H2*^{k2} *H2-T18*^{a}/SgSnJJrep (Jackson Laboratories), and F1 of B10.BR-*H2*^{k2} *H2-T18*^{a}/SgSnJJrep x MD4 mice using a previously published protocol (Miller *et al.* 2015). Briefly, mononuclear cells were isolated by Ficoll density-gradient centrifugation (Sigma-Aldrich). T-cells were removed with anti-mouse CD90.2 mAb (BD Biosciences) and guinea pig complement (Innovative Research, Inc.) and monocytes and dendritic cells by panning. B-cells were kept at 37°C and 5% CO_2 before and during experiments. All procedures involving mice were approved by the Institutional Animal Care and Usage Committee of the University of Maryland.

The A20 B-cell lymphoma line (ATCC #TIB-208) was cultured in DMEM (Lonza) supplemented with 10% of FBS (Thermo Fisher Scientific), 0.05 mM 2-mercaptoethanol (Sigma-Aldrich), 10 mM MOPS, 100 units/ml Penicillin, and 100 µg/ml streptomycin (Gemini) at 37°C and 5% CO_2.

The 3A9 T-cell hybridoma line (ATCC #CRL-3293) was cultured in DMEM (ATCC) supplemented with 5% FBS (Thermo Fisher Scientific), 0.05 mM 2-mercaptoethanol (Sigma-Aldrich) at 37°C and 5% CO_2.

Antigen-coated beads

Latex NH_2-beads (3 µm diameter, 3.5 x 10^8 beads/preparation, Polyscience) were activated with 8% glutaraldehyde in 0.5 ml PBS for 120 min under rotation at room temperature, washed with PBS, and incubated overnight with equal molar amounts of $F(ab')_2$ goat-anti-mouse IgM+G (αM, 20 µg/ml, Jackson ImmunoResearch Laboratories), hen egg lysozyme (HEL, 5.8 µg/ml,

Sigma-Aldrich), duck egg lysozyme (DEL)-I (Langley *et al.* 2017), holo-transferrin (Tf, 32 μg/ml, Sigma-Aldrich), Alexa Fluor (AF) 488-conjugated Tf (AF488-Tf, 32 μg/ml, Thermo Fisher Scientific), or AF488-F(ab')$_2$ goat-anti-mouse IgM+G (AF488-αM, 20 μg/ml, Jackson ImmunoResearch Laboratories) in 1 ml PBS. Protein content determination (BCA, Thermo Fisher Scientific) of coupling solutions before and after bead incubation confirmed that similar molar amounts of protein were conjugated in each case. The beads were then blocked with PBS 1% BSA in PBS for 30 min under rotation, washed to remove unconjugated proteins, counted in a Neubauer chamber and stored at 4°C in PBS containing 1% BSA and 5% glycerol. Streptavidin-conjugated Yellow-Green latex beads (2 μm diameter, 5 x 10^8 beads/preparation, Polyscience) were washed with 1% BSA in PBS and incubated with Biotin-SP (long spacer)-conjugated Fab fragments of goat-anti-mouse IgG (H+L) (40 μg of biotinylated antibody/mg of beads, Jackson ImmunoResearch Laboratories) for 30 min at 4°C, washed, counted in a Neubauer chamber and stored at 4°C in PBS containing 1% BSA and 5% glycerol.

Antigen-coated planar lipid bilayers (PLB)

PLB were prepared as previously described (Dustin *et al.* 2007; Liu *et al.* 2012; Spillane and Tolar 2017). Briefly, liposomes were generated from 5 mM 1,2-dioleoyl-sn-glycero-3-phosphocholine plus 1,2-dioleoyl-sn-glycero-3-phosphoethanolamine-cap-biotin (Avanti Polar Lipids) at a 100:1 molar ratio by sonication. Eight-well coverslip chambers (Lab-Tek) were incubated with liposomes for 20 min at room temperature and washed with PBS. The chambers were then incubated with 1 μg/ml streptavidin (Jackson ImmunoResearch Laboratories) for 10 min, washed, and incubated with 10 μg/ml mono-biotinylated Fab' goat-anti-IgM+G (αM-PLB)

(Liu *et al.* 2012) or the same molar amount of biotinylated Tf (16 μg/ml, Sigma-Aldrich) (Tf-PLB) for 10 min at room temperature.

Flow cytometry analysis of PM permeabilization

Mouse splenic B-cells were incubated with beads coated with αM, HEL, DEL-I or Tf in DMEM containing 6 mg/ml BSA (DMEM-BSA) at a cell:bead ratio of 1:2 (or as indicated), or with soluble $F(ab')_2$ goat-anti-mouse IgM+G (sαM, 0.5 μg/ml) for 30 min at 37°C with 5% CO_2. Propidium iodide (PI, Sigma-Aldrich) was present during the 37°C incubation as an indicator of PM permeabilization. Cells were then analyzed by flow cytometry (BD FACSCanto II) at 10,000 cell counts/sample. Bead-bound cells were identified based on their forward (FSC)- and side-scattering (SSC) properties and fluorescence intensity (FI) when using fluorescent beads (*Figure 1-figure supplement 2*). The percentages of PI+ cells among the bead-bound cell populations were quantified using FlowJo 10.1 software.

Live-cell imaging of PM permeabilization

To assess PM permeabilization by protein-coated beads, mouse splenic B-cells or a B-cell line (A20) were incubated for 30 min at 4°C in 35 mm glass-bottom dishes (MatTek) coated with poly-lysine and then with protein-coated beads at a cell to bead ratio of 1:2 for another 30 min at 4°C. Cells were washed with DMEM-BSA and imaged in a Live Cell System chamber (Pathology Devices) at 37°C with 5% CO_2 in the presence of 50 μg/ml PI (Sigma-Aldrich) and with or without 50 μM blebbistatin (Sigma-Aldrich). Images were acquired for 60 min at 1 frame/15-30 s using a spinning disk confocal microscope (UltraVIEW VoX, PerkinElmer with a

63X 1.4 N.A. oil objective). Images were analyzed using Volocity Suite (PerkinElmer) and NIH ImageJ. More than 200 cells from 3 independent experiments were analyzed for each condition.

To analyze PM permeabilization by protein-coated PLB, splenic B-cells were incubated with FM1-43FX or FM4-64FX (Thermo Fisher Scientific) in DMEM-BSA for 5 min at 4ºC, added to coverslip chambers containing mono-biotinylated Fab' goat-anti-IgM+G or biotinylated Tf tethered to PLB, and imaged immediately at 37°C with 5% CO_2 in the presence of 50 µg/ml PI and/or 10 µg/ml FM1-43FX or FM4-64FX (Thermo Fisher Scientific) using a spinning disk confocal microscope (UltraVIEW VoX, PerkinElmer with a 63X 1.4 N.A. oil objective). Images were acquired at 1 frame/6-10 s and analyzed using Volocity (PerkinElmer) and NIH ImageJ. For quantitative analysis, the mean fluorescence intensity (MFI) of FM1-43FX or FM4-64FX in a defined area was measured using Volocity (PerkinElmer). More than 270 cells from 3 independent experiments were analyzed for each condition.

Cleaved caspase-3 detection

Splenic B-cells were pretreated or not with 1 µM staurosporine (Abcam) for 24 h at 37ºC in DMEM-BSA to induce apoptosis (Diaz *et al.* 2004), exposed to αM- or Tf-beads for 30 min at 37ºC, washed, fixed with 4% paraformaldehyde (PFA), blocked with 1% BSA, and permeabilized with 0.05% saponin. Cells were then incubated with antibodies specific for cleaved caspase-3 (Asp175) (Cell Signaling Technology) followed by AF488 donkey-anti-rabbit IgG (Life Technologies) and analyzed by flow cytometry (BD FACSCanto II) at 10,000 cell counts/sample. The percentages of cells with cleaved caspase-3 staining were determined using FlowJo 10.1 software.

BCR signaling

BCR signaling was analyzed using both flow cytometry and western blotting. For flow cytometry assays, splenic B-cells from MD4 mice were pretreated or not 5 μM of the Src kinase inhibitor PP2 (Millipore) (Cheng *et al.* 2001) for 30 min at 37ºC (conditions selected not to cause B-cell toxicity) and then incubated with HEL-beads in the presence or not of the inhibitor at 37°C for 30 min. Cells were fixed with 4% PFA, permeabilized with 0.05% saponin, incubated with mouse anti-phosphotyrosine mAb (4G10, Millipore) followed by AF488-goat-anti-mouse IgG_{2b} (Thermo Fisher Scientific) secondary antibodies, and analyzed by flow cytometry (BD FACSCanto II) at 10,000 cell counts/sample. The data were analyzed using FlowJo 10.1 software.

For western blot assays, splenic B-cells from MD4 mice were pretreated or not with 10 nM of the BTK inhibitor AVL-292 (Selleckchem) (Aalipour and Advani 2013) for 30 min at 37ºC (conditions selected not to cause B-cell toxicity) and then incubated with HEL-beads in the presence or not of the inhibitor at 37°C for 30 min. Cells treated as above were lysed using RIPA buffer (150 mM $NaCl_2$, 1% of NP40, 0.5% Sodium deoxycholate, 0.1% SDS, 50 mM Tris, pH 8.0) with protease and phosphatase inhibitors (50 mM NaF, 1 mM Na_3VO_4 and 10 mM $Na_4P_2O_7$) at 4ºC. Cell lysates were run in 4-20% gradient SDS-PAGE gels (Bio-Rad) ($5x10^6$ cells/ lane) and transferred (Bio-Rad Trans-Blot transfer system) to PVDF membranes (Millipore). The membranes were blotted with rabbit anti-phospho-BTK (pBTK; Abcam) or anti-BTK (Cell Signaling Technology) followed by HRP-anti-rabbit antibody (Jackson ImmunoResearch Laboratories) and visualization using ECL substrate (Bio-Rad) and imaging (iBright FL-1500, (Thermo Fisher Scientific).

To check if signaling affected PM permeabilization, splenic B-cells from MD4 mice were pretreated or not with 5 μM PP2 (Cheng *et al.* 2001) or 10 nM AVL-292 (Aalipour and Advani 2013) for 30 min at 37ºC and then incubated with HEL-beads in the presence or not of the inhibitor and 50 μg/ml PI (Sigma-Aldrich) at 37°C for 30 min. The percentage of PI+ cells was expressed in relation to the untreated condition.

BCR and NMII polarization

BCRs on the surface of mouse splenic B-cells were stained with Cy3-Fab donkey-anti–mouse IgM+G (Jackson ImmunoResearch Laboratories) for 30 min at 4°C. Cells were then incubated with αM- or Tf-beads at 4°C for 30 min and 37°C for different lengths of time. Cells were fixed with 4% PFA, permeabilized with 0.05% saponin, and incubated with rabbit anti-phosphorylated myosin light chain 2 (pMLC2) antibodies (Cell Signaling Technology) to label activated NMII (Bresnick 1999), followed by AF633-goat-anti-rabbit IgG (Invitrogen). Cells were analyzed by confocal fluorescence microscopy (Zeiss LSM710 with a 63X 1.4 N.A. oil objective). The percentages of cells with polarization of surface labeled BCRs and activated NMII towards bead-binding sites were quantified by visual inspection. More than 300 cells from 3 independent experiments were analyzed for each condition.

PM repair assay

Mouse splenic B-cells were pretreated or not with 12 μM bromoenol lactone (BEL, Sigma-Aldrich) in DMEM-BSA for 30 min at 37ºC before and during assays to inhibit lysosomal exocytosis and PM repair (Fensome-Green *et al.* 2007). Cells were then incubated with αM-beads (1:2 cell-bead ratio) with or without inhibitors at 4ºC for 5 min and 37°C for 30 min in the

presence of FM4-64FX (Thermo Fisher Scientific), to stain wounded cells. Cells were then incubated with SYTOX™ Blue nucleic acid stain (300 nM, Invitrogen) at 4ºC for 10 min, to stain cells that failed to repair their PM tears during the 30 min incubation. Cells were analyzed by flow cytometry (BD FACSCanto II) at 10,000 cell counts/sample. Cells that were FM4-64FX positive but SYTOX Blue negative were identified as permeabilized cells that resealed. The percentages of resealed cells among total bead-bound permeabilized cells were quantified using FlowJo 10.1 software.

BCR polarization in relation to permeabilization

Surface BCRs of splenic B-cells were labeled with Cy5-Fab donkey-anti mouse IgG (Jackson ImmunoResearch) at 4ºC for 30 min. Cells were incubated with αM-PLB in the presence of FM 4-64FX (Thermo Fisher Scientific) and imaged immediately at 37°C with 5% CO_2 using a confocal spinning disk confocal microscope (UltraVIEW VoX, PerkinElmer with a 60X 1.4 N.A. oil objective). Images were acquired at 1 frame/20 s for 60 min and analyzed using a custom-made MATLAB script (MathWorks) and NIH ImageJ software. BCR polarization were analyzed using maximal projection of XZ images and quantified by the MFI ratio between defined regions within the bottom half (closer to PLB) and the top half (away from PLB) of individual cells. Cells with the bottom to top ratio ≥2 were considered polarized. More than 20 cells from 3 independent experiments were analyzed.

Lysosome exocytosis

To detect LIMP-2 exposed on the cell surface, splenic B-cells (C57BL/6 or MD4) were incubated with αM-, HEL-, DEL-I or Tf-beads for 30 min at 37°C, cooled to 4°C, and incubated

with rabbit-anti-LIMP-2 antibodies (Sigma-Aldrich) for 60 min at 4°C. Cells were then washed and fixed with 4% PFA, washed, blocked with 1% BSA in PBS and incubated with AF488 donkey-anti-rabbit IgG (Life Technologies) secondary antibodies. For intracellular LIMP-2 staining, B-cells were fixed with 4% PFA, washed, permeabilized with 0.05% saponin for 20 min, and incubated with rabbit anti-LIMP-2 antibodies followed by AF488 donkey-anti-rabbit IgG. Flow cytometry (BD FACSCanto II) was performed at 10,000 cell counts per sample. Cells were also analyzed by confocal fluorescence microscopy (Leica SPX5 with a 63X 1.4 N.A. oil objective). Polarization of LIMP-2 towards bound beads was quantified by calculating the fluorescence intensity ratio (FIR) of anti-LIMP-2 at the B-cell-bead contact site relative to the opposite side of the cell PM, using NIH ImageJ and a custom-made MATLAB script (MathWorks).

Individual events of lysosome exocytosis were captured using total internal reflection fluorescence (TIRF). Splenic B-cells were preloaded with SiR-Lysosome (1 µM, Cytoskeleton) in the presence of verapamil (10 µM, Cytoskeleton) for 30 min at 37ºC. Cells were added to coverslip chambers containing mono-biotinylated Fab' goat anti-IgM+G tethered to PLB and imaged at 37°C with 5% CO_2 in the presence of PI (50 µg/ml, Sigma-Aldrich) using a TIRF microscope (NIKON Eclipse Ti-E TIRF, 63X 1.49NA oil objective). Images were acquired at 8 frames/s during 15-20 min intervals of the 45 min incubation and analyzed using NIH ImageJ and Nikon NIS Elements software. Increases in the FI of individual SiR-Lysosome puncta (reflecting lysosome movement within the TIRF evanescent field towards the PM in contact with PLB) followed by sharp decreases within a period of 1-2 s (corresponding to a loss of the SiR-lysosome signal upon PM fusion) were scored as exocytosis events (Jaiswal *et al.* 2004). More than 20 cells were analyzed in 4 independent experiments.

Antigen internalization

For live-imaging of antigen internalization, splenic B-cells were incubated with AF488-αM-beads (1:4 cell to bead ratio) in the presence of 1 μM SiR-Lysosome and 10 μM verapamil for 30 min at 4°C, washed with DMEM-BSA and imaged by confocal fluorescence microscopy (Leica SPX5 with a 63X 1.4 N.A. oil objective) for 60 min at 1 frame/min at 37ºC. Live time-lapse images were analyzed using NIH ImageJ.

For fixed cell imaging, splenic B-cells were pretreated or not with 50 μM blebbistatin on poly-lysine coated slides for 30 min at 4°C and incubated with AF488-αM beads or AF488-Tf-beads at 37°C for varying lengths of time in the presence or not of 50 μM blebbistatin. After fixation with 4% PFA, cells were imaged by confocal fluorescence microscopy (Zeiss LSM710 with a 63X 1.4 N.A. oil objective). Percentages of cells with intracellularly-located AF488-αM puncta were determined by visual inspection of images. More than 200 cells from 3 independent experiments were analyzed for each condition.

For live-imaging of B-cells interacting with PLB, mouse splenic B-cells were added to coverslip chambers containing PLB coated with AF488-conjugated mono-biotinylated Fab' goat-anti-mouse IgM+G and incubated at 37°C with 5% CO_2 in the presence of 10 μg/ml FM 4-64FX (Thermo Fisher Scientific) for varying lengths of time. Samples were then moved to 4°C for 5 min and immediately imaged using a confocal microscope (Leica SPX5 with a 63X 1.4 N.A. oil objective). Internalization of antigen was quantified by determining the percentages of cells with intracellularly-located AF488-Fab' goat-anti-mouse IgM+G puncta in each field and by measuring the AF488 FI associated with intracellular puncta in individual cells, using a custom-made MATLAB (MathWorks) script. Cells with high FM staining were identified as wounded

and those with low FM staining as unwounded. More than 15 fields or ~90 cells from 3 independent experiments (high or low FM staining) were analyzed for each condition.

Antigen presentation and T-cell activation

To detect antigen presentation to T-cells, splenic B-cells from F1 mice of a crossing between B10.BR-*H2*^{k2} *H2-T18*^{a}/SgSnJJrep and MD4 mice were co-cultured with 3A9 T-cell hybridoma cells (ATCC® CRL-3293™) at equal concentrations (3.5×10^6 cells/ml). Cells were incubated in DMEM supplemented with 5% FBS and 0.05 mM 2-mercaptoethanol for 72 h in the presence or not of soluble HEL or DEL-I (10 µg/ml), or of beads coated with HEL, DEL-I or Tf (1:4 cell-bead ratio). After incubation, the concentration of IL-2 in the supernatant was measured using an IL-2 ELISA kit (Biolegend).

Statistical analysis

Statistical significance was assessed using unpaired, two-tailed Student's *t*-tests (Prism - GraphPad software) when only two groups were compared, and one-way ANOVA when 3 or more groups were compared. All data were presented as the mean ± SD (standard deviation).

Acknowledgments

We thank Dr. A. Upadhyaya (Department of Physics, University of Maryland) for TIRF microscopy equipment and advice, A. Beaven (CBMG Imaging Core, University of Maryland) and K. Class (CBMG Flow Cytometry Core, University of Maryland) for assistance with confocal microscopy and flow cytometry, Drs. S. K. Pierce and M. Akkaya (NIH) for the 3A9 T-cell hybridoma, and members of the Song and Andrews laboratories for helpful discussions. This

work was supported by the NIH grant R01 GM064625 to NWA and WS and NIH grant T32 GM080201 to JJHvH.

References

Aalipour, A. and Advani, R.H. (2013) Bruton tyrosine kinase inhibitors: a promising novel targeted treatment for B cell lymphomas, *Br J Haematol*, 163(4), 436-43. DOI: http://dx.doi.org/10.1111/bjh.12573.

Allen, P.M. and Unanue, E.R. (1984) Differential requirements for antigen processing by macrophages for lysozyme-specific T cell hybridomas, *J Immunol*, 132(3), 1077-9.

Allman, D. and Pillai, S. (2008) Peripheral B cell subsets, *Curr Opin Immunol*, 20(2), 149-57. DOI: http://dx.doi.org/10.1016/j.coi.2008.03.014.

Andrews, N.W., Almeida, P.E. and Corrotte, M. (2014) Damage control: cellular mechanisms of plasma membrane repair, *Trends in cell biology*, 24(12), 734-42. DOI: http://dx.doi.org/10.1016/j.tcb.2014.07.008.

Bachmann, M.F. and Jennings, G.T. (2010) Vaccine delivery: a matter of size, geometry, kinetics and molecular patterns, *Nat Rev Immunol*, 10(11), 787-96. DOI: http://dx.doi.org/10.1038/nri2868.

Bansal, D., Miyake, K., Vogel, S.S., Groh, S., Chen, C.C., Williamson, R., McNeil, P.L. and Campbell, K.P. (2003) Defective membrane repair in dysferlin-deficient muscular dystrophy, *Nature*, 423(6936), 168-72. DOI: http://dx.doi.org/10.1038/nature01573.

Batista, F.D. and Harwood, N.E. (2009) The who, how and where of antigen presentation to B cells, *Nat Rev Immunol*, 9(1), 15-27. DOI: http://dx.doi.org/10.1038/nri2454.

Batista, F.D. and Neuberger, M.S. (1998) Affinity dependence of the B cell response to antigen: a threshold, a ceiling, and the importance of off-rate, *Immunity*, 8(6), 751-9.

Batista, F.D. and Neuberger, M.S. (2000) B cells extract and present immobilized antigen: implications for affinity discrimination, *EMBO J*, 19(4), 513-20. DOI: http://dx.doi.org/10.1093/emboj/19.4.513.

Bresnick, A.R. (1999) Molecular mechanisms of nonmuscle myosin-II regulation, *Curr Opin Cell Biol*, 11(1), 26-33.

Cheng, P.C., Brown, B.K., Song, W. and Pierce, S.K. (2001) Translocation of the B cell antigen receptor into lipid rafts reveals a novel step in signaling, *J Immunol*, 166(6), 3693-701.

Cyster, J.G. (2010) B cell follicles and antigen encounters of the third kind, *Nat Immunol*, 11(11), 989-96. DOI: http://dx.doi.org/10.1038/ni.1946.

Demonbreun, A.R., Fallon, K.S., Oosterbaan, C.C., Bogdanovic, E., Warner, J.L., Sell, J.J., Page, P.G., Quattrocelli, M., Barefield, D.Y. and McNally, E.M. (2019) Recombinant annexin A6 promotes membrane repair and protects against muscle injury, *J Clin Invest*, 129(11), 4657-4670. DOI: http://dx.doi.org/10.1172/JCI128840.

Diaz, D., Prieto, A., Barcenilla, H., Monserrat, J., Prieto, P., Sánchez, M.A., Reyes, E., Hernandez-Fuentes, M.P., de la Hera, A., Orfao, A. and Alvarez-Mon, M. (2004) Loss of lineage antigens is a common feature of apoptotic lymphocytes, *J Leukoc Biol*, 76(3), 609-15. DOI: http://dx.doi.org/10.1189/jlb.0304171.

Dustin, M.L., Starr, T., Varma, R. and Thomas, V.K. (2007) Supported planar bilayers for study of the immunological synapse, *Curr Protoc Immunol*, Chapter 18, Unit 18.13. DOI: http://dx.doi.org/10.1002/0471142735.im1813s76.

Fensome-Green, A., Stannard, N., Li, M., Bolsover, S. and Cockcroft, S. (2007) Bromoenol lactone, an inhibitor of Group V1A calcium-independent phospholipase A2 inhibits antigen-stimulated mast cell exocytosis without blocking Ca2+ influx, *Cell Calcium*, 1(2), 145-53. DOI: http://dx.doi.org/10.1016/j.ceca.2006.06.002.

Fleire, S.J., Goldman, J.P., Carrasco, Y.R., Weber, M., Bray, D. and Batista, F.D. (2006) B cell ligand discrimination through a spreading and contraction response, *Science*, 312(5774), 738-41. DOI: http://dx.doi.org/10.1126/science.1123940.

Fuchs, H. and Gessner, R. (2002) Iodination significantly influences the binding of human transferrin to the transferrin receptor, *Biochim Biophys Acta*, 1570(1), 19-26.

Gitlin, A.D., Shulman, Z. and Nussenzweig, M.C. (2014) Clonal selection in the germinal centre by regulated proliferation and hypermutation, *Nature*, 509(7502), 637-40. DOI: http://dx.doi.org/10.1038/nature13300.

Gonzalez, S.F., Degn, S.E., Pitcher, L.A., Woodruff, M., Heesters, B.A. and Carroll, M.C. (2011) Trafficking of B cell antigen in lymph nodes, *Annu Rev Immunol*, 29, 215-33. DOI: http://dx.doi.org/10.1146/annurev-immunol-031210-101255.

Ibata, K., Kono, M., Narumi, S., Motohashi, J., Kakegawa, W., Kohda, K. and Yuzaki, M. (2019) Activity-Dependent Secretion of Synaptic Organizer Cbln1 from Lysosomes in Granule Cell Axons, *Neuron*, 102(6), 1184-1198.e10. DOI: http://dx.doi.org/10.1016/j.neuron.2019.03.044.

Jaiswal, J.K., Chakrabarti, S., Andrews, N.W. and Simon, S.M. (2004) Synaptotagmin VII restricts fusion pore expansion during lysosomal exocytosis, *PLoS Biol*, 2(8), E233. DOI: http://dx.doi.org/10.1371/journal.pbio.0020233.

Khan, F., Porter, M., Schwenk, R., DeBot, M., Saudan, P. and Dutta, S. (2015) Head-to-Head Comparison of Soluble vs. Qβ VLP Circumsporozoite Protein Vaccines Reveals Selective Enhancement of NANP Repeat Responses, *PLoS One*, 10(11), e0142035. DOI: http://dx.doi.org/10.1371/journal.pone.0142035.

Langley, D.B., Crossett, B., Schofield, P., Jackson, J., Zeraati, M., Maltby, D., Christie, M., Burnett, D., Brink, R., Goodnow, C. and Christ, D. (2017) Structural basis of antigen recognition: crystal structure of duck egg lysozyme, *Acta Crystallogr D Struct Biol*, 73(Pt 11), 910-920. DOI: http://dx.doi.org/10.1107/S2059798317013730.

Liu, C., Miller, H., Orlowski, G., Hang, H., Upadhyaya, A. and Song, W. (2012) Actin reorganization is required for the formation of polarized B cell receptor signalosomes in response to both soluble and membrane-associated antigens, *J Immunol*, 188(7), 3237-46. DOI: http://dx.doi.org/10.4049/jimmunol.1103065.

Liu, C.S.C. and Ganguly, D. (2019) Mechanical Cues for T Cell Activation: Role of Piezo1 Mechanosensors, *Crit Rev Immunol*, 39(1), 15-38. DOI: http://dx.doi.org/10.1615/CritRevImmunol.2019029595.

Liu, C.S.C., Raychaudhuri, D., Paul, B., Chakrabarty, Y., Ghosh, A.R., Rahaman, O., Talukdar, A. and Ganguly, D. (2018) Cutting Edge: Piezo1 Mechanosensors Optimize Human T Cell Activation, *J Immunol*, 200(4), 1255-1260. DOI: http://dx.doi.org/10.4049/jimmunol.1701118.

McNeil, P.L., Miyake, K. and Vogel, S.S. (2003) The endomembrane requirement for cell surface repair, *Proc Natl Acad Sci U S A*, 100(8), 4592-7. DOI: http://dx.doi.org/10.1073/pnas.0736739100.

Miller, H., Castro-Gomes, T., Corrotte, M., Tam, C., Maugel, T.K., Andrews, N.W. and Song, W. (2015) Lipid raft-dependent plasma membrane repair interferes with the activation of B lymphocytes, *J Cell Biol*, 211(6), 1193-205. DOI: http://dx.doi.org/10.1083/jcb.201505030.

Naegeli, K.M., Hastie, E., Garde, A., Wang, Z., Keeley, D.P., Gordon, K.L., Pani, A.M., Kelley, L.C., Morrissey, M.A., Chi, Q., Goldstein, B. and Sherwood, D.R. (2017) Cell Invasion In Vivo via Rapid Exocytosis of a Transient Lysosome-Derived Membrane Domain, *Dev Cell*, 43(4), 403-417.e10. DOI: http://dx.doi.org/10.1016/j.devcel.2017.10.024.

Natarajan, K., Sahoo, N.C. and Rao, K.V. (2001) Signal thresholds and modular synergy during expression of costimulatory molecules in B lymphocytes, *J Immunol*, 167(1), 114-22.

Natkanski, E., Lee, W.Y., Mistry, B., Casal, A., Molloy, J.E. and Tolar, P. (2013) B cells use mechanical energy to discriminate antigen affinities, *Science*, 340(6140), 1587-90. DOI: http://dx.doi.org/science.1237572.

Reddy, A., Caler, E.V. and Andrews, N.W. (2001) Plasma membrane repair is mediated by Ca(2+)-regulated exocytosis of lysosomes, *Cell*, 106(2), 157-69.

Reth, M. (1994) B cell antigen receptors, *Curr Opin Immunol*, 6(1), 3-8.

Rodríguez, A., Webster, P., Ortego, J. and Andrews, N.W. (1997) Lysosomes behave as Ca2+-regulated exocytic vesicles in fibroblasts and epithelial cells, *J Cell Biol*, 137(1), 93-104.

Sagaert, X. and De Wolf-Peeters, C. (2003) Classification of B-cells according to their differentiation status, their micro-anatomical localisation and their developmental lineage, *Immunol Lett*, 90(2-3), 179-86. DOI: http://dx.doi.org/10.1016/j.imlet.2003.09.007.

Shlomchik, M.J. and Weisel, F. (2012) Germinal center selection and the development of memory B and plasma cells, *Immunol Rev*, 247(1), 52-63. DOI: http://dx.doi.org/10.1111/j.1600-065X.2012.01124.x.

Spillane, K.M. and Tolar, P. (2017) B cell antigen extraction is regulated by physical properties of antigen-presenting cells, *J Cell Biol*, 216(1), 217-230. DOI: http://dx.doi.org/10.1083/jcb.201607064.

Spillane, K.M. and Tolar, P. (2018) Mechanics of antigen extraction in the B cell synapse, *Mol Immunol*, 101, 319-328. DOI: http://dx.doi.org/10.1016/j.molimm.2018.07.018.

Suzuki, K., Grigorova, I., Phan, T.G., Kelly, L.M. and Cyster, J.G. (2009) Visualizing B cell capture of cognate antigen from follicular dendritic cells, *J Exp Med*, 206(7), 1485-93. DOI: http://dx.doi.org/jem.20090209.

Tam, C., Idone, V., Devlin, C., Fernandes, M.C., Flannery, A., He, X., Schuchman, E., Tabas, I. and Andrews, N.W. (2010) Exocytosis of acid sphingomyelinase by wounded cells promotes endocytosis and plasma membrane repair, *J Cell Biol*, 189(6), 1027-38. DOI: http://dx.doi.org/jcb.201003053.

Vidard, L., Kovacsovics-Bankowski, M., Kraeft, S.K., Chen, L.B., Benacerraf, B. and Rock, K.L. (1996) Analysis of MHC class II presentation of particulate antigens of B lymphocytes, *J Immunol*, 156(8), 2809-18.

Villeneuve, J., Bassaganyas, L., Lepreux, S., Chiritoiu, M., Costet, P., Ripoche, J., Malhotra, V. and Schekman, R. (2018) Unconventional secretion of FABP4 by endosomes and secretory lysosomes, *J Cell Biol*, 217(2), 649-665. DOI: http://dx.doi.org/10.1083/jcb.201705047.

Wang, J., Lin, F., Wan, Z., Sun, X., Lu, Y., Huang, J., Wang, F., Zeng, Y., Chen, Y.H., Shi, Y., Zheng, W., Li, Z., Xiong, C. and Liu, W. (2018) Profiling the origin, dynamics, and function of traction force in B cell activation, *Sci Signal*, 11(542). DOI: http://dx.doi.org/10.1126/scisignal.aai9192.

Yuseff, M.I., Reversat, A., Lankar, D., Diaz, J., Fanget, I., Pierobon, P., Randrian, V., Larochette, N., Vascotto, F., Desdouets, C., Jauffred, B., Bellaiche, Y., Gasman, S., Darchen, F., Desnos, C. and Lennon-Dumenil, A.M. (2011) Polarized secretion of lysosomes at the B cell synapse couples antigen extraction to processing and presentation, *Immunity*, 35(3), 361-74. DOI: http://dx.doi.org/S1074-7613(11)00276-7.

Zhang, Z., Chen, G., Zhou, W., Song, A., Xu, T., Luo, Q., Wang, W., Gu, X.S. and Duan, S. (2007) Regulated ATP release from astrocytes through lysosome exocytosis, *Nat Cell Biol*, 9(8), 945-53. DOI: http://dx.doi.org/10.1038/ncb1620.